Supporting Information for: Plasmonic Nanopores for Trapping, Controlling Displacement, and Sequencing of DNA

Maxim Belkin,[†] Shu-Han Chao,[†] Magnus P. Jonsson,[*,‡,¶] Cees Dekker,[*,¶] and Aleksei Aksimentiev[*,†]

Department of Physics, University of Illinois at Urbana-Champaign, Organic Electronics, Department of Science and Technology (ITN), Linköping University, Sweden, and Department of Bionanoscience, Kavli Institute of Nanoscience, Delft University of Technology

E-mail: magnus.jonsson@liu.se; c.dekker@tudelft.nl; aksiment@illinois.edu

[*]To whom correspondence should be addressed
[†]University of Illinois at Urbana-Champaign
[‡]Linköping University, Sweden
[¶]Delft University of Technology

The distribution of the optical field intensity enhancement in the plasmonic nanopore system

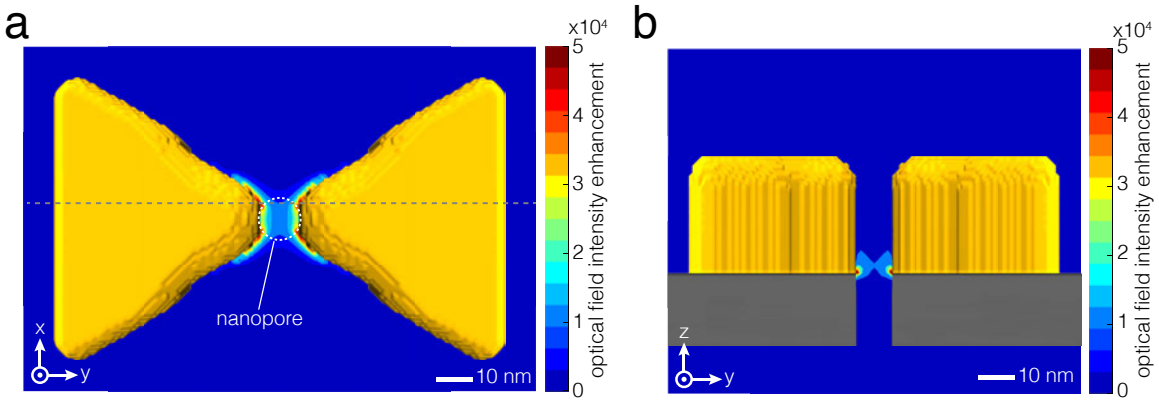

Supplementary Figure S1: The distribution of optical field intensity enhancement in the plasmonic nanopore system from FDTD calculations. (a) Top view of the plasmonic nanopore system with an x-y plane color map showing the optical field intensity enhancement distribution. The plane of the map passes through the junction of the silicon nitride membrane and the bow tie, the region where maxima of the field enhancement are observed. A 10 nm nanopore is shown by a white dashed circle. (b) Side view of the same system with a z-y plane color map showing the optical field intensity enhancement distribution at the plane cross through the tips of the gold triangles (grey dashed line in a). The plane is offset from the center of the nanopore at x direction by 3.5 nm. Two hotspots can be seen at the bow tie-membrane interface.

The effect of heat sinks on the distribution of temperature in the plasmonic nanopore system

Using the finite-element continuum simulation (COMSOL Multiphysics), we assessed the magnitude of the local temperature increase in the plasmonic nanopore systems caused by plasmonic heating. One calculation was carried out using the same bow tie geometry as in our all-atom MD simulations except that the nanopore was not present in the continuum calculations, which facilitated numerical convergence of the calculations. The total simulation volume was a cube 2 μm on each side (Figure **S2**a). The second modeling system was identical to the first one except the two diamond heat sinks ($500\times600\times40$ nm^3 each) that were present at the back side of the gold prisms (Figure **S2**b). To enable one-to-one comparison of the local temperature maps with and without the heat sinks we neglected a possible effect of the diamond blocks on plasmonic excitation. The diamond material was chosen from the COMSOL material library (named as diamond type I). The density was 3.5 g·cm^{-3} and the isobaric mass heat capacity was 0.5 J·g^{-1}K^{-1}. The Heat Transfer module was used to calculate the heat dissipation. Six boundary surfaces of the simulation box were assigned to a fixed temperature of 295 K, the same as the initial temperature of the entire system and the temperature we used in the MD simulations.

According to the previous work by Jonsson and Dekker, the maximum temperature increase in a plasmonic nanopore system of similar dimensions is $\sim$60 °C under a 10 mW laser power;[1] the local temperature increases linearly with the laser power.[2] Instead of explicitly modeling the effect of plasmonic excitation on the bow tie temperature, we considered here the bow tie as a constant heat source. The amount of heat generated by the heat source was chosen to match the previous calculations by Jonsson and Dekker. In our calculations, the local temperature between the tips of the bow tie in a steady state was 64 °C higher than the ambient temperature, Figure **S2**c. In the presence of the heat sinks and the same heat production by the plasmonic excitation, the local temperature changed more slowly and reached a steady-state temperature of only 6 °C higher than ambient temperature, Figure **S2**d. Thus, incorporation of heat sinks can indeed considerably lower the local temperature increase produced by the plasmonic heating.

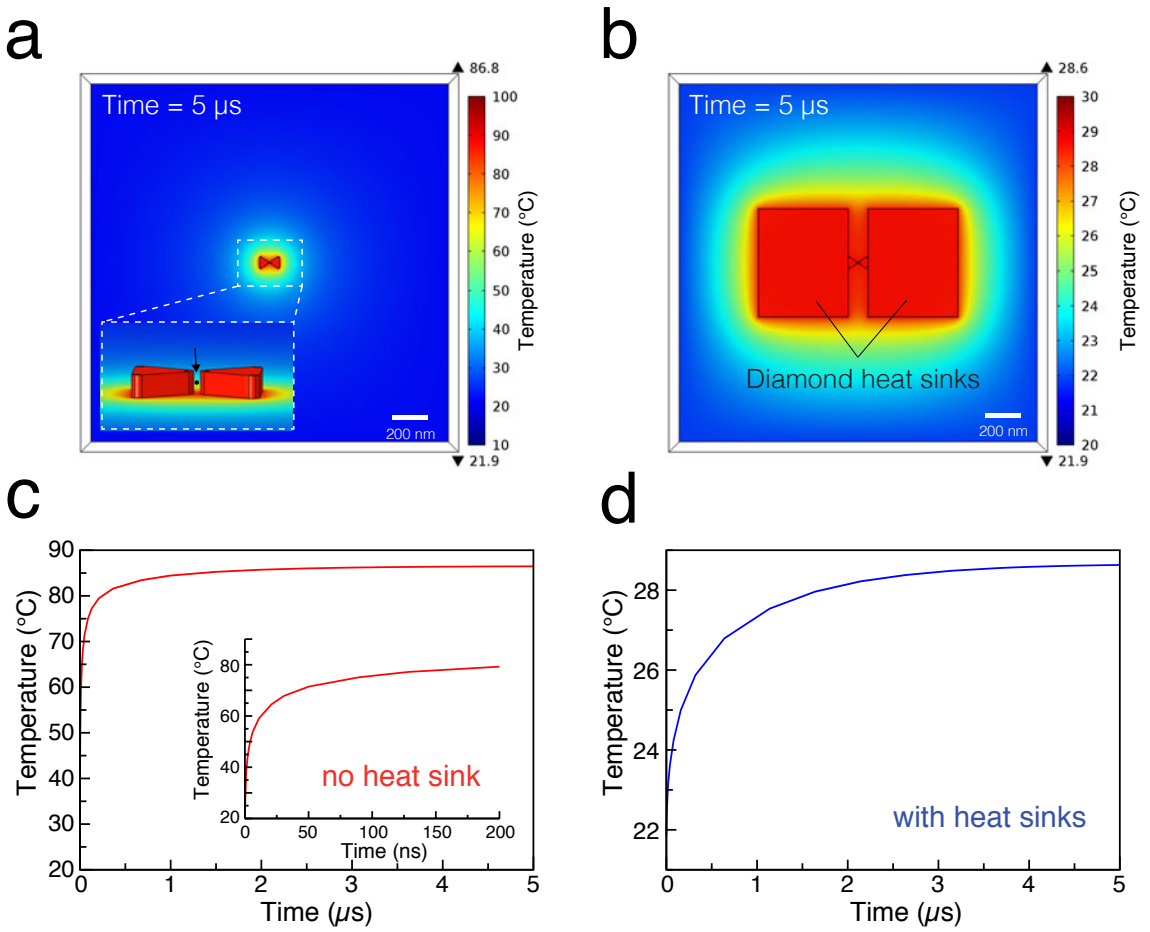

Supplementary Figure S2: Continuum model simulation of temperature distribution in the plasmonic nanopore systems. (a,b) Steady-state temperature map of two plasmonic nanopore systems featuring the same gold bow tie structure. Two $500\times600\times40$ nm^3 diamond heat sinks are present in the system characterized in panel b. Each two-dimensional temperature map characterizes the temperature distribution within the plane offset by 10 nm from the membrane surface after 5 μs of continuous plasmonic heating by a 10 kW laser beam. Note the difference in the temperature scales used in panels a and b. (c,d) Time dependence of the nanopore temperature for the two systems characterized in panels a and b. The temperature is reported at the point located between the two gold prisms 10 nm above the membrane surface; the location of this point is indicated by a black dot in the inset of panel a. The inset in panel c shows temperature change within the first 200 ns for the system containing no heat sinks.

Theoretical estimation of expected SERS signals from single DNA bases during translocation.

The total SERS signal P_{SERS} (the number of scattered photons per second) is given by:[3]

$$P_{\text{SERS}} = \sigma_{\text{effective}}\, n, \tag{1}$$

where $\sigma_{\text{effective}}$ is the effective SERS cross section of a single base and n is the number density of photons per time incident on the plasmonic structure. The latter can be estimated as the focused laser power density divided by the photon energy. Using 10 mW laser power, a beam radius of 250 nm, and a wavelength of 788 nm this gives:

$$n \approx \frac{2P\lambda}{2\pi R^2 hc} \approx \frac{2 \cdot 0.01 \cdot 788 \cdot 10^{-9}}{2\pi (250 \cdot 10^{-9})^2 \cdot 1.99 \cdot 10^{-25}} \approx 2 \cdot 10^{29} \text{photons}/(\text{m}^2\text{s}). \tag{2}$$

The effective SERS cross section $\sigma_{\text{effective}}$ can be described as:[3]

$$\sigma_{\text{effective}} \approx \frac{\sigma_{\text{local}}}{\sigma_{\text{free}}} \cdot \frac{I(\mathbf{r}, \lambda_{\text{excitation}})}{I_0} \cdot \frac{I(\mathbf{r}, \lambda_{\text{emission}})}{I_0} \approx \frac{\sigma_{\text{local}}}{\sigma_{\text{free}}} \cdot \frac{I(\mathbf{r}, \lambda_{\text{excitation}})^2}{I_0^2}, \tag{3}$$

where $I(\mathbf{r}, \lambda_{\text{excitation}})/I_0$ represents the electromagnetic field intensity enhancement at the position of the molecule of interest $\mathbf{r}$ and at a specific wavelength $\lambda_{\text{excitation}}$. Since the shift in wavelength between excitation and scattered light is small, we employ the common approximation to only use the field intensity enhancement at the excitation/laser wavelength. The first term $\sigma_{\text{local}}/\sigma_{\text{free}}$ accounts for changes of the Raman cross section of the molecule due to the presence of the substrate. This part is typically referred to as a chemical enhancement and it is strongest for adsorbed molecules. However, even for non-adsorbed molecules, the Raman polarizability may be affected by the electromagnetic field, for example, through image dipole effects.[4] The chemical enhancement is molecule-specific and typically < 10. In order to set a lower limit for detection, we, conservatively, neglect this enhancement in our estimations and use $\sigma_{\text{local}}/\sigma_{\text{free}} = 1$.

The (non-enhanced) Raman cross section of single-DNA bases can be[3] as low as 10^{-34} m^2.

Using an intensity enhancement for our structure of $\sim 10^4$ gives $\sigma_{\text{effective}}$ of $\sim 2 \cdot 10^{-24}\text{m}^2$. This finally gives a SERS signal of $\sim 10^5$ photons per second. With a state-of-the art experimental SERS setup optimized for good collection efficiency and a high signal-to-noise ratio, this should allow for rather fast (deep sub-second) acquisition times while maintaining single-base sensitivity.

We would in this respect also like to note that the possibility to optically trap the molecule during translocation in principle allows for the acquisition time to be adjusted as long as needed, in order to obtain sufficient signal-to-noise ratio. In addition, we note that have used a low estimation of $\sigma_{\text{effective}}$, and this value can probably be highly improved. For example, Kneipp *et al*. reported $\sigma_{\text{effective}}$ values of $\sim 10^{-20}$ m^2 for single DNA bases adsorbed to silver colloidal clusters.[5] In summary, our estimations show that it is realistic to expect to be able to detect single bases during translocation of a (trapped) DNA molecule.

Captions to animations

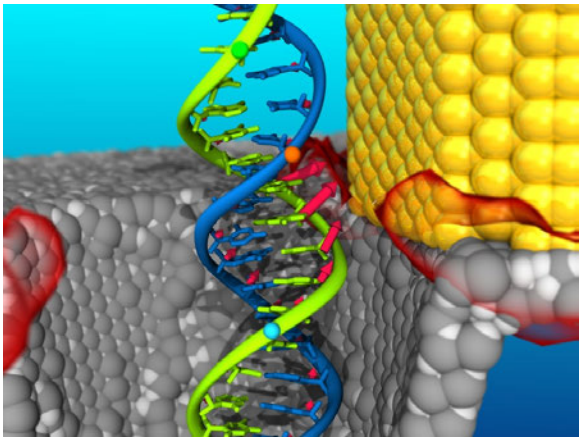

Supplementary Movie 1: Single-spot trapping of double-stranded DNA. This animation illustrates a 100 ns all-atom molecular dynamics simulation of DNA translocation through a plasmonic nanopore. The transmembrane bias is 350 mV; the plasmonic field is produced by a laser beam of 2.2 mW power. Red arrows indicate the direction and magnitude of forces experienced by individual nucleotides due to the established plasmonic fields. Semi-transparent red surfaces show the surfaces of a constant value (25,000) of the optical field enhancement potential, *i.e.* $I/I_0 = 25{,}000$. Each of the two hot spots near gold nano-triangles has "C" shape and two maxima. As a result, each hot spot appears in the movie as two semi-transparent surfaces near the corresponding tip of the gold nano-triangle.

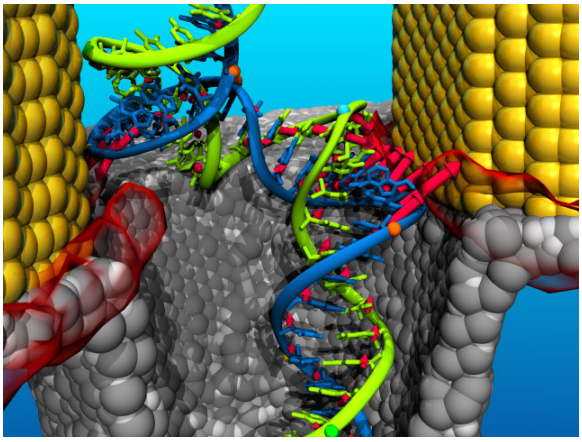

Supplementary Movie 2: Dual-spot trapping of double-stranded DNA. This animation illustrates a 100 ns all-atom molecular dynamics simulation of DNA translocation through a plasmonic nanopore. The transmembrane bias is 350 mV; the plasmonic field is produced by a laser beam of 3.7 mW power. Red arrows indicate the direction and magnitude of forces experienced by individual nucleotides due to the established plasmonic fields. Semi-transparent red surfaces show the surfaces of a constant value (25,000) of the optical field enhancement potential, *i.e.* $I/I_0 = 25{,}000$. Each of the two hot spots near gold nano-triangles has "C" shape and two maxima. As a result, each hot spot appears in the movie as two semi-transparent surfaces near the corresponding tip of the gold nano-triangle.

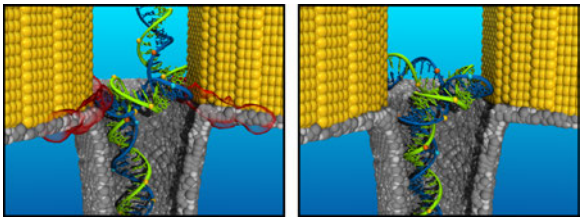

Supplementary Movie 3: Stepwise displacement of double-stranded DNA through a plasmonic nanopore. This animation illustrates a 160 ns all-atom molecular dynamics simulation of DNA translocation through a plasmonic nanopore. The transmembrane bias is 350 mV; the plasmonic field is produced by a laser beam of 3.7 mW power. The stepwise displacement is induced by periodic modulation of the laser beam. Each modulation includes the trapping and release phases. During the release phase, the plasmonic field is switched off completely and DNA is free to move through the pore. During the trapping phase, the DNA is attracted towards the plasmonic field maxima and, as a result, its motion is retarded or halted. In the movie, the duration of each phase (trapping and release) is 20 ns for a total period of the modulation cycle of 40 ns. Semi-transparent red surfaces show the surfaces of a constant value (27,000) of the optical field enhancement potential, *i.e.* $I/I_0 = 27{,}000$. Each of the two hot spots near gold nano-triangles has "C" shape and two maxima. As a result, each hot spot appears in the movie as two semi-transparent surfaces near the corresponding tip of the gold nano-triangle. Plasmonic fields are shown during the trapping phase of the modulation cycle only.

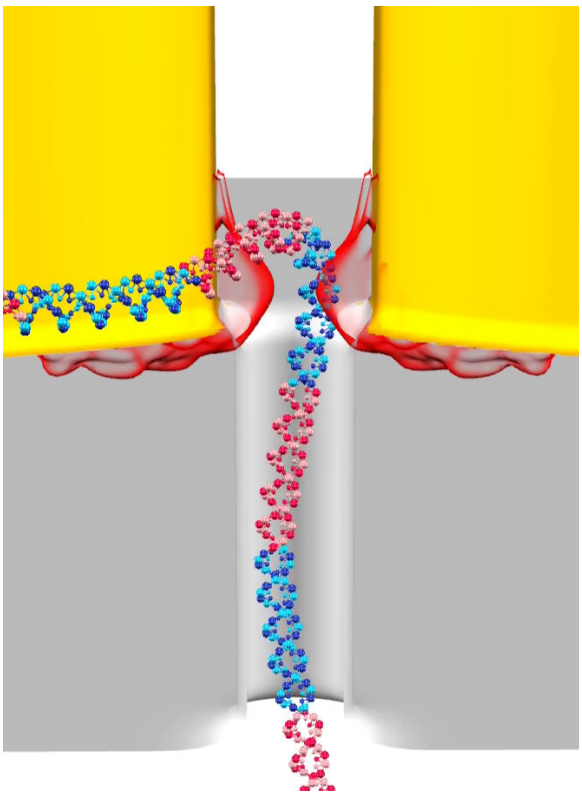

Supplementary Movie 4: Step-like motion of a double-stranded DNA molecule through the plasmonic nanopore observed in coarse-grained molecular dynamics simulations. The transmembrane bias is 50 mV; the plasmonic field is produced by a laser beam of 16.8 mW power. The step-like motion is induced by periodic modulation of the incident laser beam. Each modulation includes the on (trapping) and off (release) phases. During the off phase, the plasmonic field is switched off completely and DNA is free to move through the pore. During the on phase, the DNA is attracted towards plasmonic field maxima and, as a result, its motion is slowed down or halted. In the movie, the duration of trapping and release phases is 2.0 and 0.4 μs, correspondingly, for a total period of the modulation cycle of 2.4 μs. Semi-transparent red surfaces show the surfaces of a constant value (14,600) of the optical field enhancement potential, *i.e.* I/I_0 = 14,600. Plasmonic fields (semi-transparent red surfaces) are shown during the on phase of the modulation cycle only.

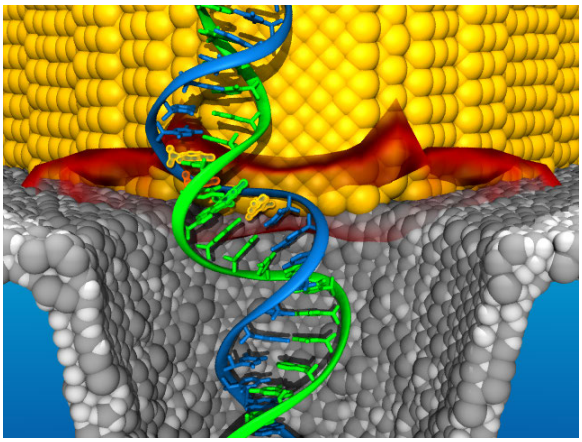

Supplementary Movie 5: Stepwise displacement of double-stranded DNA under the single hot-spot trapping conditions. This animation illustrates a 70 ns all-atom molecular dynamics trajectory. The transmembrane bias is 500 mV; the plasmonic field is produced by a laser beam of 7.4 mW power. The stepwise motion of the molecule through the nanopore is produced by a periodical modulation of the plasmonic field. The durations of the on and off phases of the plasmonic field are 5 ns each for a total period of the modulation cycle of 10 ns. Surface enhanced Raman scattering from the nucleotides in the plasmonic hot spots reports on the nucleotide composition of the DNA fragment confined to the hot spot. In the movie, the nucleotides that have major contributions to the overall SERS signal are highlighted according to their type: orange (adenin), yellow (cytosine), cyan (guanine), and green (thymine).

References

1. Jonsson, M. P.; Dekker, C. Plasmonic Nanopore for Electrical Profiling of Optical Intensity Landscapes. *Nano Lett.* **2013**, *13*, 1029–1033.

2. Nicoli, F.; Verschueren, D.; Klein, M.; Dekker, C.; Jonsson, M. P. DNA Translocations Through Solid-State Plasmonic Nanopores. *Nano Lett.* **2014**, *14*, 6917–6925.

3. Kneipp, K.; Kneipp, H. Single Molecule Raman Scattering. *Appl. Spectrosc.* **2006**, *60*, 322A–334A.

4. Le Ru, E. C.; Etchegoin, P. G. Quantifying SERS Enhancements. *MRS Bulletin* **2013**, *38*, 631–640.

5. Kneipp, K.; Kneipp, H.; Kartha, V. B.; Manoharan, R.; Deinum, G.; Itzkan, I.; Dasari, R. R.; Feld, M. S. Detection and Identification of a Single DNA Base Molecule Using Surface-Enhanced Raman Scattering (SERS). *Phys. Rev. E* **1998**, *57*, R6281–R6284.